Materials Today Bio 28 (2024) 101192

Contents lists available at ScienceDirect

Materials Today Bio

journal homepage: www.journals.elsevier.com/materials-today-bio

Engineered cyanobacteria-Fe_3O_4 hybrid system as oxygen generator and photosensitizer production factory for synergistic cancer PDT-immunotherapy

Yize Li [a,1], Yali Fan [a,1], Jin Gao [a,b,1], Shaohui Zheng [a], Yujuan Xing [a], Chunyan He [a,b], Shuo Ye [a], Hongfei Xia [a], Gezhen Wang [a], Hui Pan [a], Wei Xia [a], Meirong Sui [a], Hanjie Wang [c], Jing Liu [c,**], Manman Xie [a,***], Kai Xu [a,b,****], Yingying Zhang [a,*]

[a] School of Medical Imaging, Xuzhou Medical University, Xuzhou, 221004, China
[b] Department of Radiology, Affiliated Hospital of Xuzhou Medical University, Xuzhou, 221006, China
[c] School of Life Sciences, Faculty of Medicine, Tianjin Engineering Center of Micro-Nano Biomaterials and Detection-Treatment Technology, Tianjin Key Laboratory of Function and Application of Biological Macromolecular Structures, Tianjin University, Tianjin, 300072, China

ARTICLE INFO

Keywords:
Engineered cyanobacteria
Photodynamic therapy
Immunotherapy
Reprogramming and repolarization of M2-like TAMs

ABSTRACT

The combination of photodynamic therapy (PDT)-immunotherapy has brought much hope for cancer patients. However, the hypoxia tumor microenvironment (TME) can regulate tumor angiogenesis and inhibit immune response, thus limiting the therapeutic effects. In this paper, engineered cyanobacteria-M2-like tumor-associated macrophages (TAMs) targeting peptide modified Fe_3O_4 nanoparticles hybrid system (ECyano@Fe_3O_4-M2pep) was constructed for alleviating hypoxia and relieving immune suppression to achieve synergistic cancer PDT-immunotherapy. With the irradiation of red laser, oxygen was produced by the photosynthesis of ECyano to alleviate the hypoxia TME. Then, ECyano could secret 5-aminolevulinic acid (5-ALA) under the induction of theophylline for controllable PDT. In the process of PDT, the disulfide bond between ECyano and Fe_3O_4-M2pep was broken in response to reactive oxygen species (ROS), and then Fe_3O_4-M2pep was released to target M2-like TAMs, corresponding by the polarization of M2-like TAMs to M1-like TAMs for the killing of tumor cells. Compared with other groups, ECyano@Fe_3O_4-M2pep + theophylline + laser (ECyano@Fe_3O_4-M2pep + T + L) group displayed the lowest tumor volume (159.3 mm^3) and the highest M1/M2 ratio (1.25- fold). We believe that this hybrid system will offer a promising way for the biomedical application of bacterial therapy.

1. Introduction

Photodynamic therapy (PDT), with the advantages of minimal trauma, low toxicity, good adaptability, has become a new development direction for non-surgical treatment of malignant tumors [1]. In the process of PDT, photosensitizers (PSs) can produce reactive oxygen species (ROS) under the irradiation of specific wavelength of light, thus leading to tumor cell death [2,3]. However, the hypoxic tumor microenvironment (TME) limits the effectiveness of PDT [4]. In addition, the consumption of oxygen during PDT exacerbates the degree of hypoxia at the tumor site, thus further limiting the therapeutic effects of PDT [5]. Therefore, the sufficient oxygen supply plays an important role in improving the therapeutic effect of PDT [6].

In recent years, there have been many methods on how tumor oxygenation, such as physical oxygen loading and chemical oxygen production, can improve the therapeutic effect of PDT [7–9]. In order to improve the efficiency of oxygen supply, many oxygenic photosynthetic microorganisms [10,11] were also utilized to transport oxygen *in vivo*. Cyanobacteria, as photoautotrophic prokaryotes, have been used to generate oxygen by photosynthesis [12]. Under the irradiation of red

* Corresponding authors.
** Corresponding author.
*** Corresponding authors.
**** Corresponding author. School of Medical Imaging, Xuzhou Medical University, Xuzhou, 221004, China.
E-mail addresses: jing_liu@tju.edu.cn (J. Liu), xieman@xzhmu.edu.cn (M. Xie), xkpaper@163.com (K. Xu), zhangyy@xzhmu.edu.cn (Y. Zhang).
[1] Y. Li, Y. Fan and J. Gao contributed equally to this work.

https://doi.org/10.1016/j.mtbio.2024.101192
Received 12 May 2024; Received in revised form 4 August 2024; Accepted 5 August 2024
Available online 8 August 2024

laser, oxygen was produced by cyanobacteria to relieve tumor hypoxia [13]. PSs, including ce6 [14], indocyanine green (ICG) [15] and rose bengal (RB) [16] were combined with cyanobacteria for improved PDT. Nevertheless, due to the limited loading capacity of PSs, the therapeutic effect was barely satisfactory. With the development of synthetic biology, engineered cyanobacteria were constructed as cell factories in food industry [17], environmental protection, fuel synthesis and biomedical applications [18]. Therefore, the use of engineered cyanobacteria could not only generate oxygen, but also achieve the *in situ* production of PSs.

In addition, hypoxia stress can regulate tumor angiogenesis and inhibit immune response. Therefore, immunosuppression TME is another factor limiting PDT effect [19]. Tumor-associated macrophages (TAMs), which include anti-tumor M1-like TAMs and tumorigenic M2-like TAMs, are the most abundant innate immune cells in TME [20]. M2-like TAMs are accounted for ~70 % of TAMs, which could promote tumor growth, invasion, and metastasis [21]. The reprogramming and polarization of M2-like TAMs to M1-like TAMs could kill tumors and further improve the therapeutic effects of PDT [22]. Previous studies have shown that many receptor blockers (TLR agonists) [23], cytokines (IL-12) [24], and inorganic nanoparticles (Fe_3O_4 nanoparticles) [25] could induce the M2-to-M1 phenotype repolarization of TAMs.

Herein, engineered cyanobacteria-M2-like TAMs targeting peptide modified Fe_3O_4 nanoparticles hybrid system (ECyano@Fe_3O_4-M2pep) was developed for alleviating hypoxia and relieving immune suppression to achieve synergistic cancer PDT-immunotherapy (Scheme 1). This system was constructed by the conjugation of M2-like TAMs targeting peptide modified Fe_3O_4 nanoparticles (Fe_3O_4-M2pep) and engineered cyanobacteria (ECyano) by disulfide bonds. Under the irradiation of 640 nm laser, ECyano@Fe_3O_4-M2pep could efficiently generate abundant oxygen via photosynthesis, which can relieve tumor hypoxia and provide essential materials for PDT. Subsequently, with the addition of theophylline, 5-ALA was secreted and internalized by tumor cells to exert PDT effect with 640 nm laser irradiation. During the PDT, Fe_3O_4-M2pep were released from ECyano due to the breaking of disulfide bonds by ROS. The released Fe_3O_4-M2pep were specifically phagocyted by M2-like TAMs for repolarizing into M1-like TAMs to play anti-tumor effects. The combination of ECyano@Fe_3O_4-M2pep mediated PDT-immunotherapy could effectively inhibit tumor growth and provide a new idea for the biomedical application of cyanobacteria.

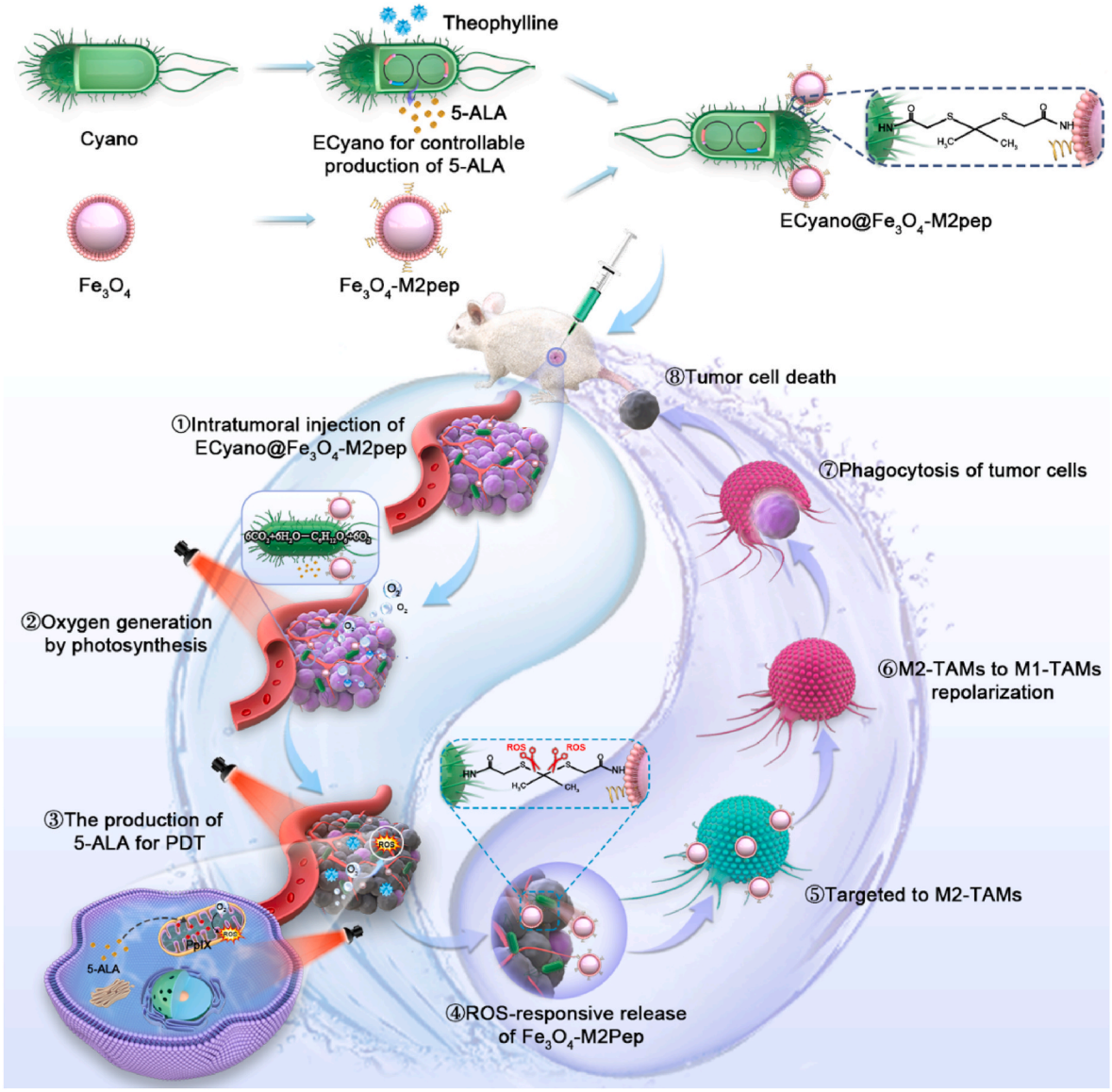

Scheme 1. The schematic illustrations of engineered cyanobacteria-Fe_3O_4 hybrid system for synergistic cancer PDT-immunotherapy.

2. Experimental section

2.1. Materials

The plasmids construction and amplification were developed in *E. coli* DH5α strain. In addition, *hemA* and *hemL* genes were synthesized (GENEWIZ, South Plainfield, NJ) for the construction of pTrc-hemA-hemL plasmid with the hema-F, hema-R and heml-F, heml-R primers, which was used for the co-expression of *hemA* and *hemL*. The vector backbone of pTrc-hemA-hemL plasmid was psI-trc-lacZ [26] and amplified using trc-R and rbcl-F primers. The pTho-hemA-hemL plasmid was used for inducible co-expression of *hemA* and *hemL*. Gene *hemA* was amplified using primers tho-hemA-F and tho-hemA-R. The primers cpc560-F and tho-cpc560-R were used to amplify the cpc560-tho induction primer using pCP3031 [26]as a template. The vector backbone was pTrc-hemA-hemL plasmid and amplified using primers spe-F and tho-heml-F. The pTrc-rhtA-ptRNA plasmid was used for the co-expression of *rhta* and the *hemB*-inhibiting ptRNA expression cassette. The gene *rhtA* was amplified using rhta-F and rhta-R primers with *E. coli* MG1655 as the template. And the synthetic hemB-inhibiting ptRNA expression cassette was amplified using primers pt-F and pt-R. The vector backbone of the plasmid pTrc-rhtA-ptRNA was pSII-pilN and amplified using pSII-R and pSII-F primers. The above sequences were assembled using ClonExpress MultiS One Step Cloning Kit (Vazyme Biotech Co., Ltd, Nanjing, China). Finally, the constructed plasmids were introduced into *Synechococcus elongatus* PCC 7942 by conjugation method. The primers and sequences used in this study were both listed in Table S1 and Table S2. The obtained ECyano strain were cultivated with BG11 medium containing 50 ng/mL of spectinomycin and 25 ng/mL of chloramphenicol with all-day light luminesce at 37 °C in a shaking incubator at 140 rpm. For 5-ALA production, 2 mM of theophylline was added to the BG11 medium. All chemical reagents were purchased from Sigma-Aldrich Chemical Reagent Co., Ltd (Shanghai, China). All cell culture associated reagents were got from GIBCO.

2.2. Cell and animal culture

Mouse breast cancer cells (4T1) and RAW264.7 macrophages were purchased from iCell Bioscience Inc (Shanghai, China) and cultured in DMEM medium containing 10 % FBS and 1 % penicillin-streptomycin. All cells were maintained at 37 °C under an atmosphere containing 5 % CO_2.

Female BALB/c mice (~20 g) were bought from the Animal Center of Xuzhou Medical University and maintained in SPF environment. All animal experiments were in accordance with legal requirements of People's Republic of China (GB14925-2010) and moral restriction. All the animal experiments were approved by the Animal Care Committee of Xuzhou Medical University (approval number:202307T031), following the principle of 3Rs (replacement, reduction, and optimization).

2.3. Construction of ECyano@Fe_3O_4-M2pep

Firstly, Fe_3O_4 nanoparticles were synthesized according to the literature [27]. Subsequently, 1 mL of Fe_3O_4 nanoparticles (1 mg/mL) were activated by reacting with 5 mg of 1-(3-Dimethylaminopropyl)-3-ethylcarbodiimide hydrochloride (EDC) and 5 mg of N-hydroxysuccinimide (NHS) for 3 h. And then, 20 μL of M2pep (1 mg/mL) was added and reacted for 2 h to obtain Fe_3O_4-M2pep nanoparticles. To achieve the responsive release of Fe_3O_4-M2pep in TME, 100 μL of 2, 2'-[PRopane-2,2-diylbis(thio)]diacetic acid (HOOC-TK-COOH, 1 mg/mL) was introduced. Fe_3O_4-M2pep-TK-COOH were obtained by dialysis (10 kDa, 24 h) and centrifugation. In the end, 5 mg of EDC and 5 mg of NHS were added to Fe_3O_4-M2pep-TK-COOH solutions and stirred for 3 h. Then, 10 mL of ECyano strain solution (3×10^8 CFU/mL) was added and reacted under lighting conditions for 12 h. Then, ECyano@Fe_3O_4-M2pep were collected by centrifuging at 3000 rpm for 5 min. The content of Fe_3O_4-M2pep in ECyano@Fe_3O_4-M2pep hybrid system was measured by phenanthroline.

2.4. Characterization

The morphologies of Fe_3O_4, Fe_3O_4-M2pep, ECyano and ECyano@-Fe_3O_4-M2pep were observed by transmission electron microscopy (TEM, FEI Tecnai G2 F30). The scanning electron microscope (SEM) images of ECyano, ECyano@Fe_3O_4-M2pep and ECyano@Fe_3O_4-M2pep after incubation with 0.3 % H_2O_2 for 4 h were acquired by Field emission scanning electron microscope (FEI Tecnai Spirit G2 Twin). The size distribution and surface zeta potentials were determined by a Zetasizer Nano ZS90 (Malvern Instruments Ltd, Malvern, UK).

2.5. Growth curves

10 μL of ECyano and ECyano@Fe_3O_4-M2pep were inoculated with 20 mL of BG11 medium overnight. Then, 200 μL of bacterial solution was taken at the cultivated time points of 0 h, 24 h, 48 h, 72 h, 96 h, 120 h, and the absorbance at 750 nm was measured by a multimode reader (BioTek Epoch, Service Card). To investigate whether the addition of theophylline affected the growth of ECyano, 0.36 mg/mL of theophylline was added.

2.6. Oxygen generation

The cyanobacteria solutions (OD_{750} = 1) were irradiated with or without 0.25 W/cm^2 of 640 nm laser for 6 min. Then the oxygen content was measured by a dissolved oxygen analyzer. In addition, the oxygen concentration of ECyano@Fe_3O_4-M2pep with 640 nm laser irradiation was also measured to study whether the hybrid of Fe_3O_4-M2pep affected the photosynthesis of ECyano.

2.7. Measurement of 5-ALA

The production of 5-ALA was measured by high-performance liquid chromatography (HPLC). The specific experimental steps were as follows: ECyano were centrifuged at 3000 rpm for 10 min, and the supernatant was collected. Then, the supernatant (80 μL) was mixed with 320 μL of $NaHCO_3$ solution (0.2 M) and 400 μL of dansyl chloride acetonitrile solution (10 mM). The mixture was cultured at 30 °C for 30 min, which was stopped by adding 800 μL of hydrochloric acid (0.12 M). After filtering, samples were subjected to Waters 2695 HPLC (Waters Corporation, Milford, MA, USA) equipped with an Venusil MP C18 column (5 μm, 4.6 mm × 150 mm). The mobile phase was acetonitrile-water (pH 6.0, 25:75, v/v) containing 50 mM potassium phosphate, and the flow rate was set 0.8 mL/min.

2.8. In vitro PDT effects of ECyano@Fe_3O_4-M2pep

2.8.1. CCK8 assay

The cytotoxic effects of 5-ALA mediated PDT were firstly explored. 4T1 cells were cultured with different concentrations of 5-ALA standards for 24 h. 0.25 W/cm^2 of 640 nm laser was exposed to study the PDT mediated cell killing effects. And the cytotoxic effects of ECyano@-Fe_3O_4-M2pep mediated PDT were also investigated. 100 μL of ECyano or ECyano@Fe_3O_4-M2pep and 100 μL of theophylline (3.6 mg/mL) were added to induce the production of 5-ALA. After 20 h of incubation, cells were irradiated by 0.25 W/cm^2 of 640 nm laser for 10 min, and then incubated for another 4 h. Then, CCK8 reagent was added and the OD_{450} values were measured by a multimode reader (BioTek Epoch, Service Card).

2.8.2. Intracellular ROS detection

DCFH-DA probe was used to investigate the ROS generation. 1×10^5

of 4T1 cells were inoculated into the lower chamber of transwell (0.4 μm). Subsequently, 1 mL of cyanobacterial cells (3x10^8 CFU/mL) were placed into the upper chamber and co-cultured for 20 h. 100 μL of theophylline (3.6 mg/mL) was additionally added to induce the production of 5-ALA. Then cells were irradiated with 0.25 W/cm^2 of 640 nm laser for 10 min, stained with DCFH-DA probe for 15 min, washed with PBS and imaged under an inverted fluorescence microscope (Leica DMI3000 B, Germany).

2.8.3. In vitro hypoxia relief

To validate the effect of O_2 generated in the process of photosynthesis on hypoxia in TME, luminescent oxygen sensor $Ru(dpp)_3Cl_2$ was selected. 4T1 cells were inoculated into the lower chamber of transwell (0.4 μm) in hypoxia incubator. Subsequently, 1 mL of ECyano cells (3 × 10^8 CFU/mL) were placed in the upper chamber and co-cultured for 4 h. 100 μL of theophylline (3.6 mg/mL) was additionally added to induce the production of 5-ALA. Then cells were irradiated with 0.25 W/cm^2 of 640 nm laser for 10 min, stained with DAPI and $Ru(dpp)_3Cl_2$ probe for 30 min, and imaged by a confocal laser microscope (Leica STELLARIS 5, Germany).

2.8.4. Calcein-AM/PI staining

To intuitive embody the PDT effect, Calcein-AM/PI assay was used to indicate the dead cells. 4T1 cells and cyanobacteria were separately inoculated into the lower and upper chamber of transwell (0.4 μm) for 20 h. Then cells were irradiated with 0.25 W/cm^2 of 640 nm laser for 10 min, stained with calcein-AM and PI probe for 10 min, and imaged under an inverted fluorescence microscope (Leica DMI3000 B, Germany).

2.8.5. Cell apoptosis analysis

4T1 cells and cyanobacteria were separately inoculated into the lower and upper chamber of transwell (0.4 μm) for 20 h. Then cells were irradiated with 0.25 W/cm^2 of 640 nm laser for 10 min, stained with Annexin V-FITC/PI kits for 15 min, and subjected to flow cytometry (FACS CantonII).

2.9. In vitro assessment of M2-like macrophage polarization

2.9.1. In vitro cellular uptake study

RAW264.7 cells were treated with 20 ng/mL of IL-4 for 24 h to obtain M2-like macrophage. Firstly, M2-like macrophages were incubated with different concentrations of Fe_3O_4 and Fe_3O_4-M2pep for 24 h to study the cytotoxicitic effects. Besides, the cell viability of 4T1 cells incubated with different concentrations of Fe_3O_4-M2pep for 24 h was also evaluated. Then, M2-like macrophages were cultured with 75 μg/mL of Fe_3O_4 and Fe_3O_4-M2pep for 4 h, washed with PBS, stained with prussian blue kits and observed by an inverted fluorescence microscope (Leica DMI3000 B, Germany).

In order to testify the ROS responsive release behavior of Fe_3O_4-M2pep from ECyano@Fe_3O_4-M2pep, RAW264.7 cells were seeded into the lower chamber of transwells (0.4 μm) and treated with 20 ng/mL of IL-4 for 24 h to obtain M2-like macrophage. Subsequently, 1 mL of Fe_3O_4-M2pep, ECyano, ECyano@Fe_3O_4-M2pep (equivalent to 75 μg of Fe_3O_4-M2pep and 3 × 10^8 CFU of ECyano) were placed in the upper chamber and co-cultured for 4 h. Then 2 μL of H_2O_2 solution with different concentrations was added to simulate ROS within TME in ECyano@Fe_3O_4-M2pep group. After 4 h, M2-like macrophages were washed, stained and observed by an inverted fluorescence microscope (Leica DMI3000 B, Germany).

2.9.2. In vitro polarization of M2-like to M1-like macrophage

Firstly, M2-like macrophages were treated with 75 μg/mL of Fe_3O_4 and Fe_3O_4-M2pep for 8 h, washed with PBS, stained with anti-CD86-PE and anti-CD206-FITC antibodies at 4 °C in the dark for 1 h and measured by flow cytometry (FACS CantonII). The cell supernatant was collected to measure the contents of iNOS, TNF-α, TGF-β and IL-10 using ELISA kits according to manufacturer's instructions.

In order to verify the released Fe_3O_4-M2pep from ECyano@Fe_3O_4-M2pep for the polarization of M2-like macrophage, M2-like macrophages were seeded into the lower chamber of transwell (0.4 μm). Subsequently, 1 mL of Fe_3O_4-M2pep (75 μg), ECyano (3 × 10^8 CFU), ECyano@Fe_3O_4-M2pep (equivalent to 75 μg of Fe_3O_4-M2pep and 3 × 10^8 CFU of ECyano) were placed in the upper chamber and co-cultured for 8 h. Then 2 μL of H_2O_2 solution (0.3 %) was added to simulate ROS within TME in ECyano@Fe_3O_4-M2pep group. At last, cells were harvested, washed, stained with anti-CD86-PE and anti-CD206-FITC and detected by flow cytometry (FACS CantonII). The contents of iNOS, TNF-α, TGF-β and IL-10 in cellular supernatants were also measured.

2.9.3. The phagocytosis of M1-like macrophage

M2-like macrophages were treated with 75 μg/mL of Fe_3O_4 and Fe_3O_4-M2pep for 8 h, followed by staining with anti-CD11b-Cy5.5 at 4 °C in the dark for 1 h. And then 4T1 cells were stained with 1 μM of DID at 37 °C for 30 min. And then, the obtained M1-like macrophages were cultured with 4T1 cells for 6 h, detected and analyzed by flow cytometry (FACS CantonII).

2.10. In vivo biosafety study

Female BALB/c mice (20 g) were randomly divided into four groups (n = 3): PBS; Fe_3O_4-M2pep; ECyano; ECyano@Fe_3O_4-M2pep. 200 μL of PBS, Fe_3O_4-M2pep, ECyano and ECyano@Fe_3O_4-M2pep were intravenously injected, respectively. Besides, the amounts of Fe_3O_4-M2pep and ECyano in all groups were 75.1 μg and 3 × 10^8 CFU/mouse. After 21 days, mice were sacrificed and blood was collected for blood routine and biochemical analysis. Major organs (heart, liver, spleen, lung and kidney) were harvested for HE staining.

2.11. The assessment of in vivo PDT effect

4T1 subcutaneous tumor model was established to investigate the PDT-immunotherapy effect of ECyano@Fe_3O_4-M2pep. Mice were randomly divided into five groups (n = 3): control group (intratumoral injection of PBS), ECyano@Fe_3O_4-M2pep group (intratumoral injection of ECyano@Fe_3O_4-M2pep, 50 μL), ECyano@Fe_3O_4-M2pep group + T group (intratumoral injection of ECyano@Fe_3O_4-M2pep with the addition of theophylline, 50 μL), ECyano@Fe_3O_4-M2pep group + L group (intratumoral injection of ECyano@Fe_3O_4-M2pep with 640 nm laser irradiation, 50 μL), ECyano@Fe_3O_4-M2pep group + T + L group (intratumoral injection of ECyano@Fe_3O_4-M2pep with the addition of theophylline and 640 nm laser irradiation, 50 μL). Besides, the amounts of Fe_3O_4-M2pep and ECyano in all groups were 75.1 μg and 3 × 10^8 CFU/mouse. After injection of ECyano@Fe_3O_4-M2pep, ECyano@Fe_3O_4-M2pep + L group and ECyano@Fe_3O_4-M2pep + T + L group were exposed to 640 nm red laser (0.25 W cm^{-2}, 5 min) for three consecutive days to exert photosynthetic oxygen production. On the 4th day, mice in ECyano@Fe_3O_4-M2pep + T group and ECyano@Fe_3O_4-M2pep + T + L group received an oral gavage of 2 mM theophylline solution to induce the secretion of 5-ALA. And 640 nm red laser (0.25 W cm^{-2}, 10 min) was given to mice in ECyano@Fe_3O_4-M2pep + L and ECyano@Fe_3O_4-M2pep + T + L group on the 5^{th} day. On 1^{st}, 3^{rd}, and 5^{th} day, tumor tissues were harvested to study the *in vivo* survival of ECyano. The body weight and tumor volume were recorded every other day. After 21 days' treatment, tumor tissues were collected for H&E, TUNEL and HIF-1α immunohistochemical staining. Besides, the biodistribution of ECyano@Fe_3O_4-M2pep in main organs, blood and tumor tissues were studied by measuring the Fe content.

2.12. In vivo polarization of TAMs

Tumor tissues were collected, digested, filtered and stained with anti-mouse F4/80-APC, anti-mouse CD86-PE and anti-mouse CD206-

FITC antibodies at 4 °C for 1 h, and then cells were detected by flow cytometry. In addition, tumor cells were lysed and the supernatants were collected for the detection of iNOS and IL-10. In the end, tumor tissues slices were stained with anti-mouse F4/80-APC, anti-mouse CD86-PE, anti-mouse CD206-FITC and DAPI for immunofluorescence assay.

2.13. In vivo transcriptome high throughput sequencing

Mice in control and ECyano@Fe_3O_4-M2pep + T + L groups were sacrificed and tumor tissue was collected for RNA extraction. The RNA samples were sent to ANOROAD Co., Ltd. for gene sequencing. Heatmap was plotted by https://www.bioinformatics.com.cn (last accessed on Nov 10, 2023), an online platform for data analysis and visualization.

2.14. Statistical analysis

These data were represented as mean ± SEM (n ≥ 3). All data were processed by GraphPad Prism 9. Statistical analysis was performed using Student's t-test, one-way analysis of variance (ANOVA) or two-way ANOVA method. When $^{*}P < 0.05$, the differences were significant, and when $^{**}P < 0.01$, the differences were very significant.

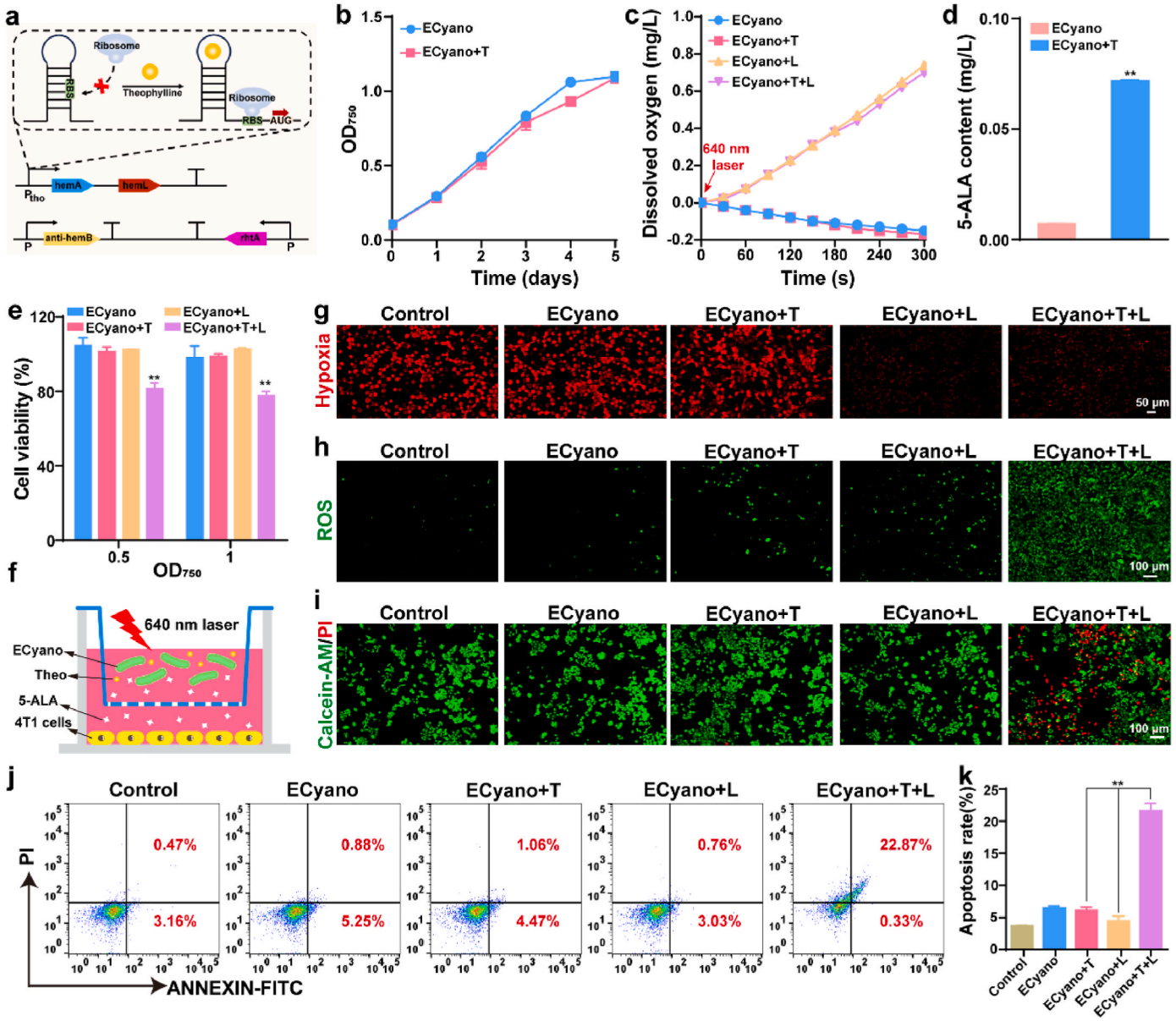

Fig. 1. Characterization of ECyano. a: The construction of ECyano; b: Growth curves of ECyano with or without theophylline supply; c: The photosynthetic oxygen evolution of ECyano with or without theophylline supply under 640 nm red laser irradiation; d: The generation and secretion of 5-ALA induced by theophylline, $^{**}P < 0.01$ compared with ECyano group by Student's t-test; e: Cell viabilities of 4T1 cells incubated with the supernatants of ECyano in different conditions, $^{**}P < 0.01$ compared with ECyano group by one way ANOVA; f: The scheme of transwell assay; g: Measurements of hypoxia of 4T1 cells in different groups (scale bar: 50 μm); h: The ROS detection in 4T1 cells with different treatments (scale bar: 100 μm); i: Cell live/dead staining (scale bar: 100 μm); j: Cell apoptosis of 4T1 cells in different groups; k: Quantitative analysis of the ratio of apoptosis cells. $^{**}P < 0.01$ compared with ECyano + T and ECyano + L groups by one way ANOVA. ECyano + T, ECyano induced by theophylline to produce 5-ALA; ECyano + L, ECyano under 640 nm laser irradiation; ECyano + T + L, ECyano treated with theophylline and 640 nm laser.

3. Results and discussion

3.1. The controllable secretion of 5-ALA from ECyano

In order to achieve the *in vivo* controllable production of 5-ALA, recombinant plasmids were introduced into *Synechococcus elongatus* PCC 7942 to construct ECyano. As shown in Fig. 1a, two key genes *hemA* and *hemL* separately encoded glutamyl-tRNA reductase (GluTR) and glutamate-1-semialdehyde 2,1-aminomutase (GSA-AM). And the expressions of GluTR GSA-AM were controlled by theophylline-responsive riboswitch, which could catalyze glutamal-RNA to 5-ALA [28]. In order to achieve the secretion of 5-ALA into the extracellular space, *rhtA* gene encoded L-threonine/L-homoserine exporter as transport proteins, which could transport 5-ALA to the extracellular space [29]. Besides, *hemB* gene encoded porphobilinogen synthase to inhibit the expression of hemB, thus increasing the production of 5-ALA.

To verify whether the addition of theophylline could influence the growth of ECyano, the growth curves of ECyano and ECyano + T (ECyano induced by theophylline to produce 5-ALA) were measured as illustrated in Fig. 1b. ECyano and ECyano + T displayed similar growth behaviors, demonstrating that the addition of theophylline could not influence the growth of ECyano. In addition, the oxygen generation in photosynthesis is an important factor in alleviating the hypoxia TME and enhancing the PDT effects. In our previous studies [30], 0.25 W/cm^2 of 640 nm laser could induce the photosynthesis and not influence the normal growth. As shown in Fig. 1c, compared with no laser irradiation groups, the dissolved oxygen significantly increased in ECyano + L (ECyano under 640 nm laser irradiation) and ECyano + T + L groups (ECyano treated with theophylline and 640 nm laser), providing a foundation for improving tumor hypoxia.

Afterwards, the controllable generation and secretion of 5-ALA in ECyano induced by theophylline were testified and the results were shown in Fig. 1d. ECyano + T group revealed the higher content of 5-ALA than that in ECyano group.

These data showed that ECyano was successfully constructed and 5-ALA could be produced and released under the induction of theophylline, laying the foundation for subsequent verification of PDT effects.

3.2. The in vitro PDT effect of ECyano

In order to evaluate the *in vitro* PDT effects of ECyano, a series of assays were conducted. As we know, 5-ALA is a second-generation photosensitizer developed in recent years, which is a precursor of photosensitizer with no fluorescence. After exogenous 5-ALA enters tumor cells, it can be converted into protoporphyrin IX (PpIX), which is a highly photosensitive substance that undergoes PDT with red light irradiation [31]. First of all, 4T1 cells were incubated with 5-ALA standards and ECyano + T to study the generation of PpIX (Fig. S1a). Compared with control group, there were red fluorescence in 5-ALA and ECyano + T groups, indicating that 5-ALA could be produced and released under the induction of theophylline. Subsequently, the cytotoxity of 5-ALA mediated PDT was measured by CCK8 assay (Fig. S1b). When the concentration of 5-ALA reached to 160 μg/mL, the cell viability decreased from 87.1 % to 29.0 % after 640 nm laser exposure. In addition, the cell viability with laser irradiation displayed a concentration-dependent manner. Similarly, the cytotoxicity of ECyano against 4T1 cells was also assessed (Fig. 1e). In the absence of irradiation, ECyano exhibited excellent biocompatibility on 4T1 cells, and the addition of 2 mM theophylline had almost no effect on cell viability. However, in the presence of theophylline and 640 nm laser irradiation (0.25 W/cm^2, 10 min), the cell viability obviously decreased, indicating that the generation of 5-ALA induced by theophylline could be used for killing tumors by PDT.

Subsequently, a transwell system (Fig. 1f), which contained ECyano in the upper chamber and tumor cells in the lower chamber, was designed to further verify the *in vitro* PDT function of ECyano. The generation of oxygen by photosynthesis could be used for alleviating tumor hypoxia, and the production of 5-ALA could be uptaken by tumor cells for PDT. Firstly, the alleviation of hypoxia was detected by a hypoxia-sensitive fluorescence probe $Ru(dpp)_3Cl_2$. As show in Fig. 1g, ECyano and ECyano + T groups displayed similar red fluorescence to control group, indicating that there was no oxygen generation in the absence of 640 nm laser irradiation. The red fluorescence intensity in ECyano + L group was significantly lower than that in control group, showing the alleviation effect of oxygen generated in the process of photosynthesis. While the red fluorescence intensity of ECyano + T + L group was higher than that in ECyano + L group, which was because the oxygen consumption in PDT further exacerbated the hypoxia in TME.

As we known, the generation of ROS in PDT could exert anti-tumor effect. Therefore, DCFH-DA probe was used for ROS detection. As shown in Fig. 1h and Fig. S2, there were negligible green fluorescence in control, ECyano, ECyano + T and ECyano + L groups, while ECyano + T + L group exhibited the highest green fluorescence. This phenomenon was attributed to 5-ALA mediated PDT, and the generation of oxygen can further provide components for PDT to induce more ROS production.

Calcein-AM/PI and cell apoptosis assays were used for testing the cellular killing effect. As displayed in Fig. 1i, there were no vivid red fluorescence in control, ECyano, ECyano + T and ECyano + L groups. More excitingly, ECyano + T + L group represented the highest ratio of dead cells, which was in accordance with the cytotoxic and ROS generation results. Soon afterwards, flow cytometry was used to quantitatively analyze the apoptosis rates. As shown in Fig. 1j and k, the apoptosis rates in control, ECyano, ECyano + T and ECyano + L groups were 3.63 %, 6.13 %, 5.53 % and 3.79 %, separately. While the apoptosis rate in ECyano + T + L (22.7 %) was greatly augmented, which was consistent with the live/dead cell staining results.

All these above data demonstrated that ECyano treated with theophylline and 640 nm laser could induce the generation of ROS, thus inducing tumor cell death.

3.3. Characterization of Fe_3O_4-M2pep

According to the previously published literature [25], Fe_3O_4 nanoparticles with diameter of ~20 nm were incubated with macrophages, followed by the upregulation of M1-related markers (TNFα and CD86) and downregulation of M2-related markers (CD206 and IL10). Related data demonstrated that Fe_3O_4 nanoparticles could significantly inhibit tumour growth by inducing M2-like macrophages towards M1-like macrophage subtype, which was due to the cellular iron regulating functional plasticity in macrophages. In this paper, M2 targeting peptide (M2pep) was modified with Fe_3O_4 nanoparticles (Fig. 2a) to achieve the targeted delivery. As displayed in Fig. 2b, Fe_3O_4 and Fe_3O_4-M2pep were spherical and displayed the particle sizes of about 15.4 ± 1.9 nm and 17.6 ± 1.6 nm, respectively. DLS results demonstrated that the hydrodynamic diameters of Fe_3O_4 and Fe_3O_4-M2pep were 51 ± 0.5 nm and 68 ± 2.1 nm (Fig. 2c). The zeta potentials of Fe_3O_4 and Fe_3O_4-M2pep were −16.5 mV and −8.8 mV, respectively (Fig. S3), indicating the successful conjugation of M2pep to Fe_3O_4.

3.4. The targeting ability of Fe_3O_4-M2pep

To achieve the polarization of M2-like TAMs in TME, the biocompatibilities of Fe_3O_4 and Fe_3O_4-M2pep on M2-like macrophages were firstly measured by CCK-8 assay. Firstly, the *in vitro* generation of M2-like macrophages was verified by flow cytometry (Fig. S4). Cell viabilities in both Fe_3O_4 and Fe_3O_4-M2pep groups were higher than 80 % when the concentration was lower than 75 μg/mL (Fig. 2d). To further evaluate the cytotoxicity of Fe_3O_4-M2pep on tumor cells, CCK8 assay was conducted to study the killing effect of Fe_3O_4-M2pep on 4T1 cells, and the results were shown in Fig. S5. When the concentration of Fe_3O_4-M2pep was 100 μg/mL, the cell viability was higher than 85 %,

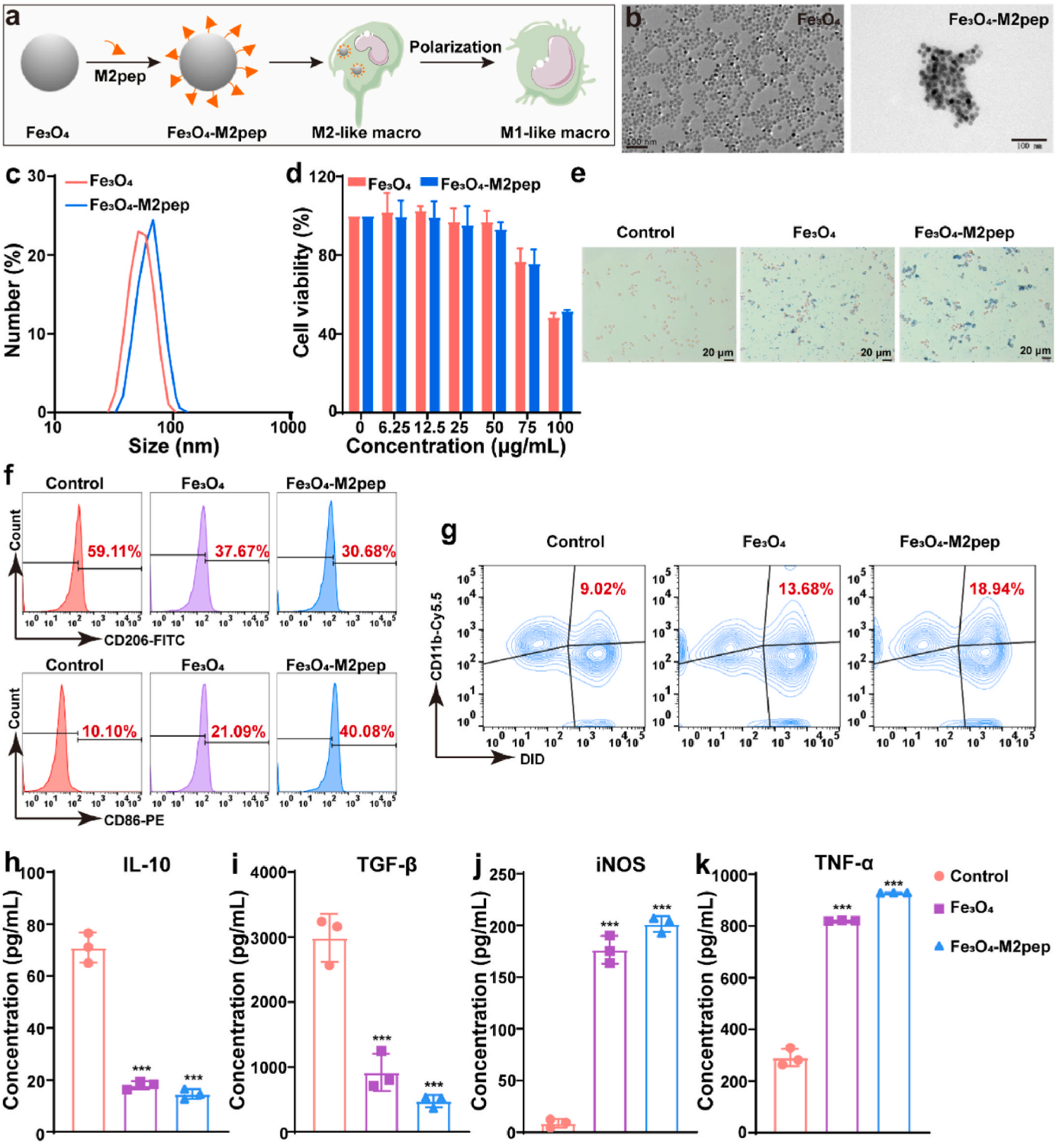

Fig. 2. Characterization of Fe_3O_4-M2pep. a: Scheme of Fe_3O_4-M2pep synthesis and the polarization of M2-like macrophages to M1-like macrophages; b: TEM images of Fe_3O_4 and Fe_3O_4-M2pep (scale bar: 100 nm); c: Size distribution of Fe_3O_4 and Fe_3O_4-M2pep; d: Cell viabilities of M2-like macrophages incubated with different concentrations of Fe_3O_4 and Fe_3O_4-M2pep for 24 h; e: Prussian blue staining of M2-like macrophages incubated with 75 μg/mL of Fe_3O_4 and Fe_3O_4-M2pep for 4 h (scale bar: 20 μm); f: Flow cytometric analysis of the polarization of M2-like macrophages in different groups; g: Validation of M1-like macrophages phagocytosis of tumor cells induced by Fe_3O_4-M2pep (DID: 4T1 cells, CD11b-Cy5.5: M1-like macrophages). Measurement of IL-10 (h), TGF-β (i), iNOS (j) and TNF-α (k) in cell supernatants by ELISA kits. ***$P < 0.001$ compared with control group by one way ANOVA.

demonstrating that Fe_3O_4-M2pep had good biological safety.

Subsequently, M2pep mediated targeting ability was checked by Prussian blue staining assay. The cytoplasm and intercellular iron could be stained pink and blue with 1 % nuclear fixation red and Prussian blue, respectively. As shown in Fig. 2e and Fig. S6, the iron content in Fe_3O_4-M2pep group (0.44 mg/L) was higher than that in Fe_3O_4 group (0.36 mg/L), indicating that the addition of M2pep could increase the cellular uptake of Fe_3O_4, laying the foundation for subsequent *in vitro*

polarization experiments.

3.5. The in vitro polarization performance of M2-like macrophages

To study the polarization effect of Fe_3O_4-M2pep, CD86 and CD206 were selected as the characteristic biomarkers of M1-like and M2-like macrophages, respectively. As shown in Fig. 2f and Fig. S7a, the percentages of $CD206^+$ M2-like macrophages in Fe_3O_4 and Fe_3O_4-M2pep groups were 37.67 % and 30.68 %, which were significantly lower than control group (59.11 %). In addition, the percentages of $CD86^+$ M1-like macrophages in control, Fe_3O_4 and Fe_3O_4-M2pep groups were 10.10 %, 21.09 % and 40.08 %, separately. What's more, Fe_3O_4-M2pep group displayed the highest ratio of M1-like macrophages and the lowest ratio of M2-like macrophages, which was mainly due to the targeting ability and the increased cellular uptake of Fe_3O_4-M2pep. Notably, the ratio of M1/M2-like macrophages in Fe_3O_4-M2pep group was 1.83- fold of that in Fe_3O_4 group (Fig. S7b), indicating that the introduction of M2pep could improve the polarization efficiency of M2-like macrophages. Subsequently, the phagocytosis effect of M1-like macrophages on tumor cells was studied. As shown in Fig. 2g and Fig. S8, there were 13.68 % and 18.94 % of tumor cells phagocytosed by M1-like macrophages in Fe_3O_4 and Fe_3O_4-M2pep groups.

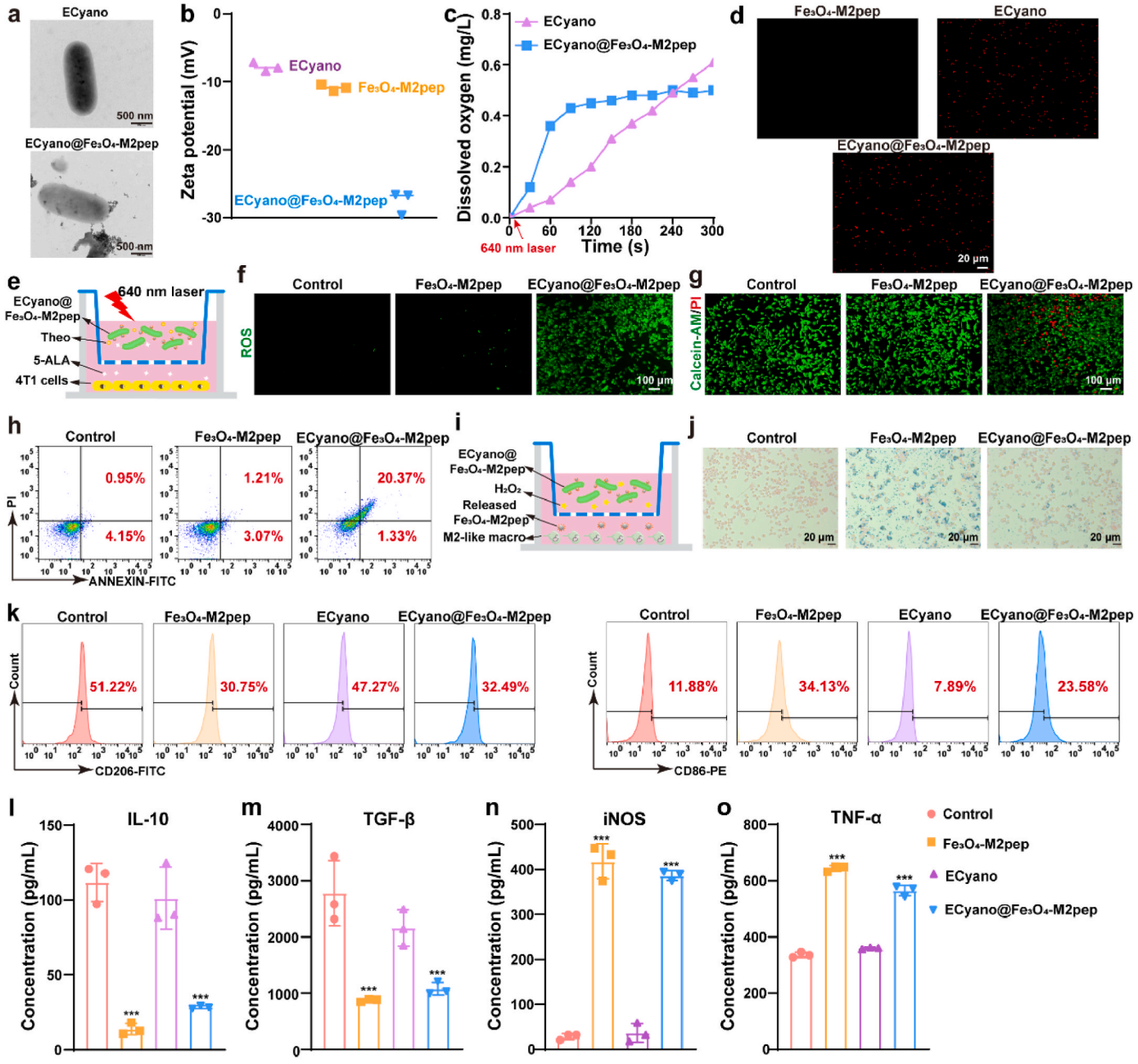

Fig. 3. Characterization of ECyano@Fe_3O_4-M2pep. a: TEM images of ECyano and ECyano@Fe_3O_4-M2pep (scale bar: 500 nm); b: Zeta potentials of ECyano, Fe_3O_4-M2pep and ECyano@Fe_3O_4-M2pep; c: The photosynthetic oxygen evolution of ECyano and ECyano@Fe_3O_4-M2pep under 640 nm red laser irradiation; d: Fluorescence images of ECyano, Fe_3O_4-M2pep and ECyano@Fe_3O_4-M2pep excited by 561 nm (scale bar: 20 μm); e: The scheme of transwell assay for PDT; f: The ROS detection in 4T1 cells with different treatments (scale bar: 100 μm); g: Live/dead staining of 4T1 cells (scale bar: 100 μm); h: Cell apoptosis analysis; i: The scheme of transwell assay for M2-like macrophages polarization; j: Prussian blue staining of M2-like macrophages in the lower chamber of transwell (scale bar: 20 μm); k: Flow cytometric analysis of the polarization of M2-like macrophages in different groups; Measurement of IL-10 (l), TGF-β (m), iNOS (n) and TNF-α (o) in cell supernatants by ELISA kits. $^{***}P < 0.001$ compared with control group by one way ANOVA.

In the end, ELISA assay was conducted to further indicate the *in vitro* polarization performance. IL-10 and TGF-β cytokines were secreted by M2-like macrophages, iNOS and TNF-α cytokines were secreted by M1-like macrophages. Therefore, the concentrations of IL-10, TGF-β, iNOS and TNF-α were measured by ELISA kits. As shown in Fig. 2h and i, the concentrations of IL-10 and TGF-β in Fe_3O_4 and Fe_3O_4-M2pep groups were significantly lower than control group. While the concentrations of iNOS and TNF-α in Fe_3O_4 and Fe_3O_4-M2pep groups were significantly higher than control group (Fig. 2j and k). These data further validated the augmented polarization effect of M2-like macrophages to M2-like macrophages.

3.6. Characterization of ECyano@Fe_3O_4-M2pep

To achieve the synergistic effect of PDT and immunotherapy, Fe_3O_4-M2pep were conjugated to the surface of ECyano by the ROS-responsive linker (HOOC-TK-COOH) to prepare ECyano@Fe_3O_4-M2pep. In the process of ECyano mediated PDT, ROS was generated and then Fe_3O_4-M2pep were released and target M2-like TAMs, there by inducing the polarization to further kill tumor cells. Fig. 3a showed the TEM images of ECyano and ECyano@Fe_3O_4-M2pep, suggesting that Fe_3O_4-M2pep were successfully modified with ECyano. In order to further test and verify the construction of ECyano@Fe_3O_4-M2pep, compared with ECyano, there were some nanoparticles adsorbed on the surface of ECyano in ECyano@Fe_3O_4-M2pep (Fig. S9). Additionally, the zeta potentials of ECyano, Fe_3O_4-M2pep and ECyano@Fe_3O_4-M2pep were −7.8 mV, −10.9 mV and −27.6 mV, respectively (Fig. 3b), further indicating the successful preparation of ECyano@Fe_3O_4-M2pep.

Furthermore, the bacterial activity and photosynthetic oxygen of ECyano@Fe_3O_4-M2pep were characterized. As shown in Fig. 3c, the oxygen production rate in ECyano@Fe_3O_4-M2pep group was increased in the first 4 min of red laser exposure. And the initial oxygen generation was slightly lower than ECyano, indicating that the modification of Fe_3O_4-M2pep did not significantly affect the photosynthesis. This phenomenon may be due to an increase in electron transfer after being connected to nanoparticles, leading to an increase in oxygen production rate [32]. However, this increase in oxygen production rate will bring certain metabolic pressure to ECyano itself, leading to a decrease in the upper limit of oxygen production capacity. Fluorescence images (Fig. 3d) of chlorophyll in ECyano and ECyano@Fe_3O_4-M2pep groups indicated that the modification of Fe_3O_4-M2pep had no influence on the bacterial activity.

These results proved the successful preparation of ECyano@Fe_3O_4-M2pep and the bacterial activity and oxygen-producing function was not affected.

3.7. The in vitro PDT effect of ECyano@Fe_3O_4-M2pep

The *in vitro* PDT effect of ECyano@Fe_3O_4-M2pep was assessed by CCK8 assay, ROS detection, Calcein-AM/PI staining and apoptosis analysis by a transwell system (Fig. 3e). ECyano@Fe_3O_4-M2pep were placed in the upper chamber and 4T1 cells were seeded in the lower chamber. When 4T1 cells were incubated with ECyano@Fe_3O_4-M2pep, the cell viability significantly decreased after red laser exposure (Fig. S10). As shown in Fig. 3f and Fig. S11, the green fluorescence in ECyano@Fe_3O_4-M2pep was significantly higher than that in Fe_3O_4-M2pep and control groups, declaring that 5-ALA was generated, secreted and transported to 4T1 cells in the lower chamber for PDT. Subsequently, calcein-AM/PI staining assay was used to evaluate the PDT effects (Fig. 3g). The red fluorescence (dead cells) in ECyano@Fe_3O_4-M2pep group was the highest, which was due to the large amount of ROS generated. Similarly, the apoptosis rate in ECyano@Fe_3O_4-M2pep group was 21.7 %, which was clearly higher than that in Fe_3O_4-M2pep (4.28 %) and control (5.1 %) groups (Fig. 3h and Fig. S12).

3.8. The polarization of M2-like macrophage induced by ECyano@Fe_3O_4-M2pep

To measure the polarization effect, we firstly evaluated whether Fe_3O_4-M2pep could release from ECyano. Specifically, ECyano@Fe_3O_4-M2pep were placed in the upper chamber and M2-like macrophages were seeded in the lower chamber with a 0.4 μm filter (Fig. 3i). We firstly evaluated the release behavior of Fe_3O_4-M2pep from ECyano under the conditions of different H_2O_2 content. As shown in Fig. S13, with the increase of H_2O_2 content, more Fe_3O_4-M2pep were uptaken by M2-like macrophages in the lower chamber, demonstrating that more Fe_3O_4-M2pep were released, transported to the lower chamber and ingested by M2-like macrophages. Therefore, 0.3 % of H_2O_2 solution was added to the upper chamber to stimulate TME. In ddition, the SEM image of ECyano@Fe_3O_4-M2pep after incubation with 0.3 % of H_2O_2 solution for 4 h was provided in Fig. S14. Some Fe_3O_4-M2pep nanoparticles released from ECyano, demonstrating the disulfide bond between ECyano and Fe_3O_4-M2pep broken under the H_2O_2 environment. In the end, Fig. 3j and Fig. S15 illustrated the Prussian blue staining of M2-like macrophages in the lower chamber to visualize intracellular iron content. The iron contents in Fe_3O_4-M2pep group (0.438 mg/L) and ECyano@Fe_3O_4-M2pep (0.309 mg/L) were significantly higher than that in control group. And ECyano@Fe_3O_4-M2pep group owned the similar Fe content to Fe_3O_4-M2pep group, indicating that Fe_3O_4-M2pep could release and target M2-like macrophages.

Secondly, the polarization induced by ECyano@Fe_3O_4-M2pep was also assessed by flow cytometry and ELISA. As shown in Fig. 3k and Fig. S16a, the percentages of M2-like macrophages in Fe_3O_4-M2pep and ECyano@Fe_3O_4-M2pep groups were 30.75 % and 32.49 %, which were lower than that in control (51.22 %) and ECyano (47.27 %) groups. On the contrary, the proportions of M1-like macrophages in Fe_3O_4-M2pep and ECyano@Fe_3O_4-M2pep groups were 34.13 % and 23.58 %, which were higher than that in control (11.88 %) and ECyano (7.89 %) groups. In addition, the ratio of M1-like macrophages in ECyano@Fe_3O_4-M2pep group was lower than Fe_3O_4-M2pep group, which was probably due to the incomplete release of Fe_3O_4-M2pep from ECyano. Notably, the ratios of M1/M2-like macrophages in Fe_3O_4-M2pep and ECyano@Fe_3O_4-M2pep group were 1.04- and 0.68- fold of that in control group (Fig. S16b), indicating that ROS-responsive released Fe_3O_4-M2pep in the upper chamber could pass through the transwell system and target M2-like macrophages to induce the polarization. The measurement of immune factors (Fig. 3l–o) was also in accordance with the flow cytometric results.

These above data proved that the modification of Fe_3O_4-M2pep could not affect the function of ECyano for PDT and Fe_3O_4-M2pep could release during the PDT process for causing the polarization of M2-like macrophages to M1-like macrophages.

3.9. In vivo therapeutic effect of ECyano@Fe_3O_4-M2pep

Lastly, 4T1 subcutaneous tumor model was established to investigate the PDT-immunotherapy effect of ECyano@Fe_3O_4-M2pep. Mice were randomly divided into five groups (n = 3): control group, ECyano@Fe_3O_4-M2pep group, ECyano@Fe_3O_4-M2pep group + T group, ECyano@Fe_3O_4-M2pep group + L group, ECyano@Fe_3O_4-M2pep group + T + L group. After injection of ECyano@Fe_3O_4-M2pep, ECyano@Fe_3O_4-M2pep + L group and ECyano@Fe_3O_4-M2pep + T + L group were exposed to 640 nm red laser for three consecutive days to exert photosynthetic oxygen production. On the 4^{th} day, mice in ECyano@Fe_3O_4-M2pep + T group and ECyano@Fe_3O_4-M2pep + T + L group received an oral gavage of 2 mM theophylline solution to induce the secretion of 5-ALA. And 640 nm red laser (0.25 W cm^{-2}, 10 min) was given to mice in ECyano@Fe_3O_4-M2pep + L and ECyano@Fe_3O_4-M2pep + T + L groups on the 5th day (Fig. 4a).

In order to validate the viability of ECyano within the treatment period, tumor tissues in ECyano@Fe_3O_4-M2pep + T + L group were

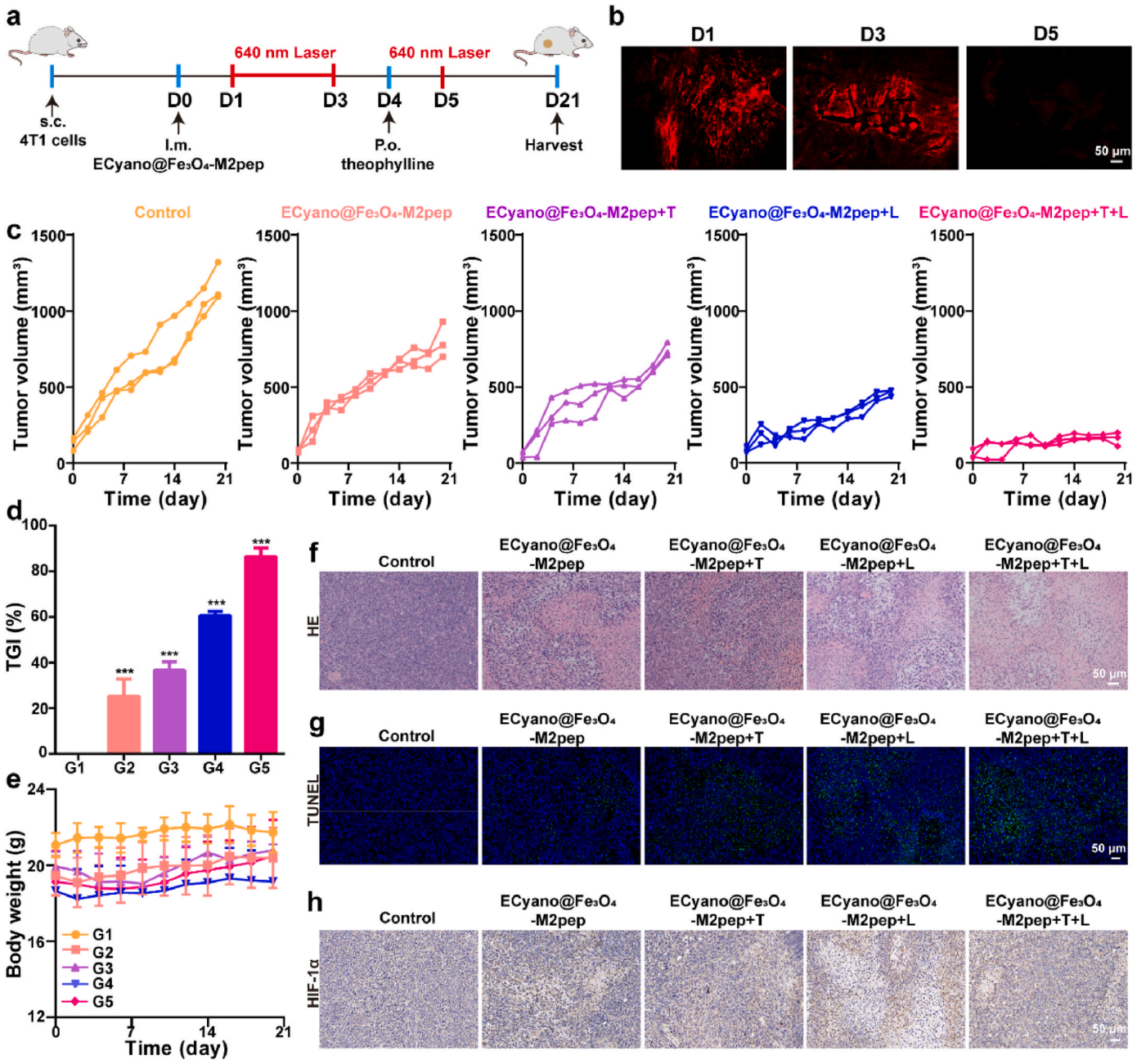

Fig. 4. ***In vivo*** **anti-tumor effects of ECyano@Fe_3O_4-M2pep.** a: Schedule of animal experiments; b: Fluorescence images of tumor tissue sections excited by 561 nm; c: Changes of tumor volumes in different groups (scale bar: 1 cm); d: Tumor growth inhibition (TGI) rates in different groups; e: Body weight changes of mice during the treatment; f: HE staining of tumor tissues; g: TUNEL staining of tumor tissues; h: Immunohistochemical analysis of HIF-1α expression. Scale bar: 50 μm.

collected on 1st, 3rd, and 5th days to observe the red fluorescence of chlorophyll. As shown in Fig. 4b, the red fluorescence on 1st and 3rd days was vivid. Due to the fact that the production of 5-ALA was controlled by theophylline, the red fluorescence on 1st and 3rd days indicated the existence of living ECyano. On the 5th day, weak red fluorescence appeared in tumor tissues, which may be the luminescence from PpIX converted by 5-ALA. During the treatment period, the tumor growth curves and photos of excised tumors were shown in Fig. 4c and Fig. S17. After the treatment, the average tumor volumes in control, ECyano@Fe_3O_4-M2pep, ECyano@Fe_3O_4-M2pep + T, ECyano@Fe_3O_4-M2pep + L and ECyano@Fe_3O_4-M2pep group + T + L groups were 1174 mm^3, 801 mm^3, 745 mm^3, 463 mm^3 and 159 mm^3, respectively. Compared with ECyano@Fe_3O_4-M2pep + T group and ECyano@Fe_3O_4-M2pep + L group, ECyano@Fe_3O_4-M2pep group + T + L group displayed the smallest tumor volume, which was attributed to the synergistic effect of 5-ALA mediated PDT and Fe_3O_4-M2pep mediated immunotherapy. In addition, the tumor volume in ECyano@Fe_3O_4-M2pep + T group was similar to that in ECyano@Fe_3O_4-M2pep group, illustrating that the addition of theophylline could only induce the generation of 5-ALA. Besides, the tumor growth inhibition (TGI) rate in ECyano@Fe_3O_4-M2pep group + T + L group was the highest (Fig. 4d), which was consistent with the above results.

Besides, the biodistribution of ECyano@Fe_3O_4-M2pep was studied by measuring the Fe contents in main organs (heart, liver, spleen, lung, kidney), blood and tumor tissues. As shown in Fig. S18, there was no significant difference in the Fe contents in heart, liver, spleen, lung, kidney and blood between control and ECyano@Fe_3O_4-M2pep groups. However, the Fe contents in tumor of ECyano@Fe_3O_4-M2pep group was

0.35 mg/L, which was significantly higher than that in control group (0.009 mg/L). This data demonstrated that intratumoral injection of ECyano@Fe_3O_4-M2pep was mainly accumulated in tumor tissues, ensuring the good biosafety. More importantly, the overall body weight gain, blood routine, blood biochemistry analysis and HE staining of main organs also indicated the biological safety of ECyano@Fe_3O_4-M2pep (Fig. 4e and Fig. S19).

At last, tumor tissues were collected for hematoxylin-eosin (H&E) and TdT-mediated dUTP Nick-End Labeling (TUNEL) staining to evaluate the tumor cells apoptosis. In comparison with control group, the tumor tissues of ECyano@Fe_3O_4-M2pep group + T + L group were not so dense and nucleus were disrupted, indicating that the tumor growth was inhibited (Fig. 4f). TUNEL method was used to measure the tumor apoptosis. As shown in Fig. 4g and Fig. S20, the green fluorescence intensity in ECyano@Fe_3O_4-M2pep group + T + L group was the highest, indicating that most tumor cells have undergone apoptosis. ECyano@Fe_3O_4-M2pep group + T group and ECyano@Fe_3O_4-M2pep group + L group displayed the similar green fluorescence, lower than that in ECyano@Fe_3O_4-M2pep group + T + L group. This phenomenon was attributed to synergistic effect of PDT and immunotherapy.

Due to the photosynthetic oxygen production of ECyano, the alleviation of tumor hypoxia was estimated by HIF-1α (a typical hypoxia marker) immunohistochemical staining assay. Compared with control group, the expression of HIF-1α was decreased in ECyano@Fe_3O_4-

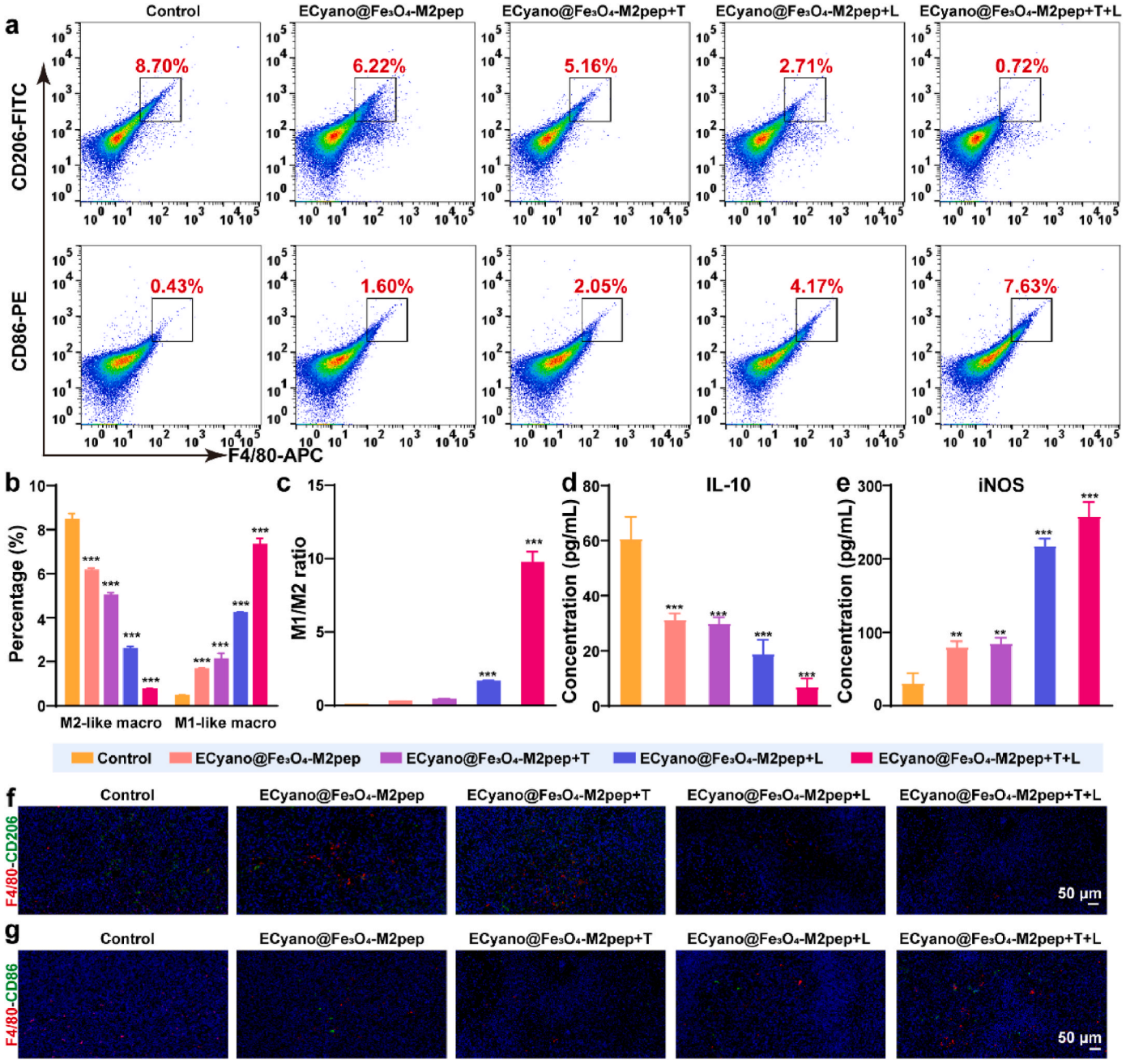

Fig. 5. *In vivo* polarization of M2-like TAMs. a: Flowcytometric analysis of M2-like TAMs and M1-like TAMs in tumor tissues; b: The percentages of M2-like TAMs and M1-like TAMs; ***$P < 0.001$ compared with control group by two-way ANOVA. c: The ratios of M1/M2-like TAMs in different groups; Measurement of IL-10 (d), and iNOS (e) in tumor tissues by ELISA kits; f: Immunofluorescence analysis of F4/80 and CD206 expression to indicate the M2-like TAMs in tumor tissues (scale bar: 50 μm); g: Immunofluorescence analysis of F4/80 and CD86 expression to indicate the M1-like TAMs in tumor tissues (scale bar: 50 μm). ***$P < 0.001$, **$P < 0.01$ compared with control group by one way ANOVA.

M2pep + L group, which was owing to the photosynthesis of ECyano (Fig. 4h and Fig. S21). While the aggravated hypoxia was found in ECyano@Fe_3O_4-M2pep + T + L group, which was induced by the oxygen consumption in the process of PDT.

3.10. In vivo polarization of M2-like TAMs

The *in vivo* polarization of M2-like TAMs to M1-like TAMs was further investigated using flow cytometry (Fig. 5a). Compared with control group (the ratios of M2-like TAMs and M1-like TAMs were 8.70 % and 0.43 %), both ECyano@Fe_3O_4-M2pep and ECyano@Fe_3O_4-M2pep + T groups displayed the decreased M2-like TAMs (the percentages were 6.22 % and 5.16 %) and increased M1-like TAMs (the proportions were 1.60 % and 2.05 %), which was owing to the disruption of ROS-responsive linker between ECyano and Fe_3O_4-M2pep caused by the high levels of ROS in TME, leading to targeted uptake of Fe_3O_4-M2pep by M2-like TAMs for polarizing into M1-like TAMs. Above all, ECyano@Fe_3O_4-M2pep + T + L group demonstrated the lowest M2-like TAMs and the highest M1-like TAMs (Fig. 5b). Notably, the M1/M2 ratios in ECyano@Fe_3O_4-M2pep + L and ECyano@Fe_3O_4-M2pep + T + L groups were separately 1.14- and 1.25- fold (Fig. 5c), which were significantly higher than that in control (0.27- fold), ECyano@Fe_3O_4-M2pep (0.53- fold) and ECyano@Fe_3O_4-M2pep + T (0.69- fold) groups.

Similarly, the concentrations of IL-10 and iNOS were measured and the results kept peace with the flow cytometric results. As shown in Fig. 5d and e, ECyano@Fe_3O_4-M2pep + T + L group possessed the lowest IL-10 content (secreted by M2-like TAMs) and the highest iNOS concentration (secreted by M1-like TAMs).

In the end, tumor tissues were collected and stained with anti-F4/80, anti-CD206 and anti-CD86 antibodies to analyze the changes of M2-like and M1-like TAMs. As displayed in Fig. 5f and g, the green fluorescence intensity of CD206 in ECyano@Fe_3O_4-M2pep + T + L group was lower than any other groups, and the green fluorescence intensity of CD86 was higher than any other groups.

These data demonstrated that Fe_3O_4-M2pep could release from ECyano, alleviate the immunosuppressive TME, and enhance the therapeutic effects.

3.11. Mechanism of enhanced PDT-immunotherapy

To study the mechanism of ECyano@Fe_3O_4-M2pep mediated enhanced PDT-immunotherapy, transcriptomic analysis of tumor issues was conducted. As shown in Fig. 6a–c, there were 385 significantly differentially expressed genes (DEGs) in control and ECyano@Fe_3O_4-

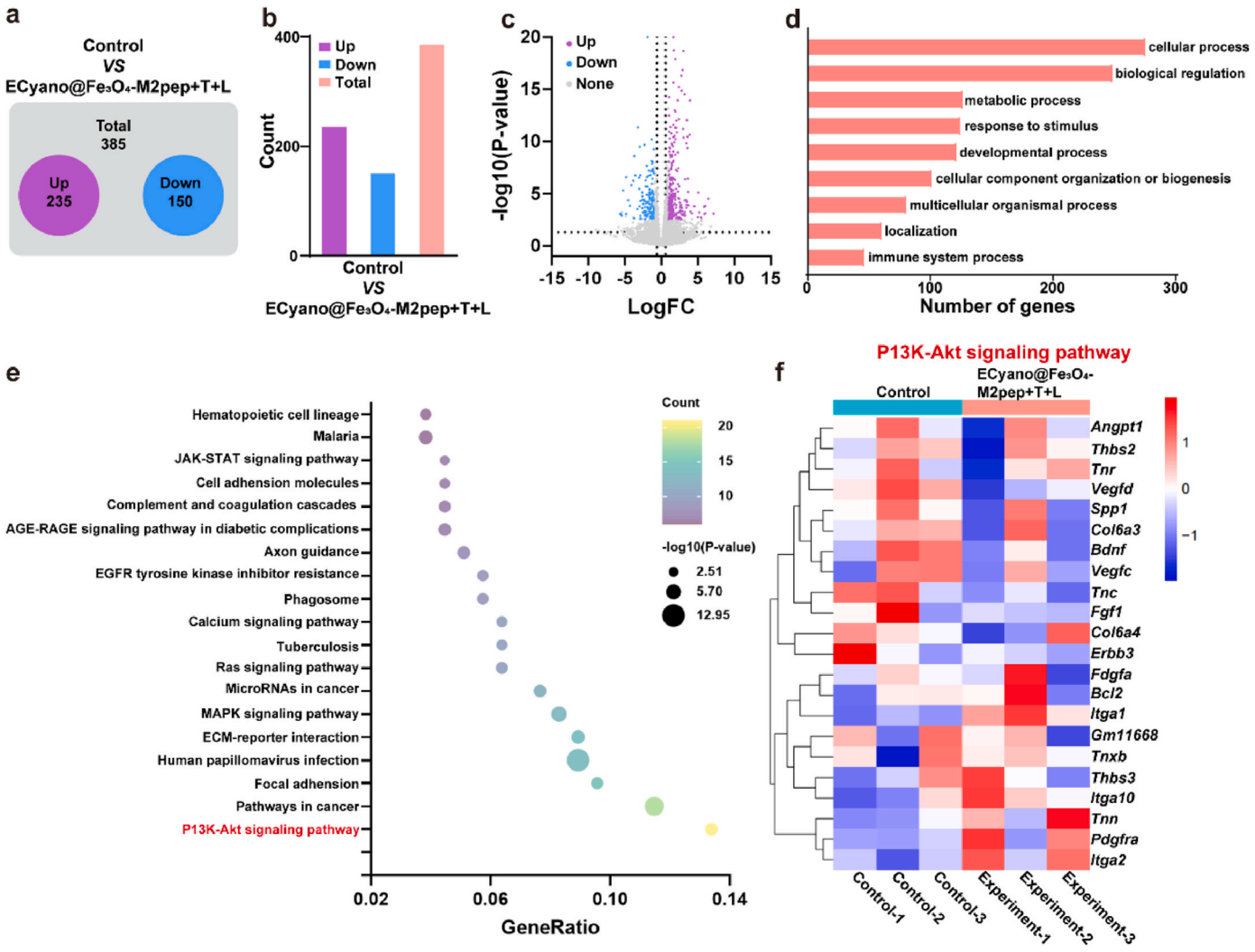

Fig. 6. Mechanism of ECyano@Fe_3O_4-M2pep mediated therapy. a: Venn diagram of transcriptomic profiles; b: The differential expressed genes (DEGs) in control and ECyano@Fe_3O_4-M2pep + T + L groups; c: The volcano map of identified DEGs in control and ECyano@Fe_3O_4-M2pep + T + L groups; d: GO enrichment analysis of biological processes in ECyano@Fe_3O_4-M2pep + T + L group; e:KEGG pathway enrichment analysis of the identified DEGs inECyano@Fe_3O_4-M2pep + T + L group; f: The heat map of the DEGs in PI3K-AKT signaling pathway after ECyano@Fe_3O_4-M2pep + T + L treatment.

M2pep + T + L groups, which included 235 up-regulation and 150 down-regulation genes. Subsequently, the biological functions of DEGs were analyzed by gene ontology (GO) enrichment. As displayed in Fig. 6d, cellular process and biological regulation mainly led to the difference in the biological functions of DEGs. To further demonstrate the biological functions of DEGs, Kyoto Encyclopedia of Genes and Genomes (KEGG) pathway enrichment were performed in Fig. 6e and f. Among them, the gene ratio of phosphatidylinositol 3-kinase (PI3K-Akt) signaling pathway was the highest. According to the published works [33], the PI3K-AKT signaling network regulated by growth factors directly regulates nutrient transporters and metabolic enzymes, or controls transcription factors that regulate the expression of key components in metabolic pathways, thereby disconnecting the control of tumor cell growth, survival, and metabolism from exogenous growth stimuli. The PI3K-Akt signaling pathway can be activated by the production of intracellular ROS, leading to tumor cell apoptosis. Therefore, ECyano@Fe_3O_4-M2pep mediated PDT-immunotherapy could activate PI3K-Akt signaling pathway, thus induing tumor cell death.

Although ECyano@Fe_3O_4-M2pep has achieved some progress, but there are still some issues that need to be addressed. Different from other micro/nano-materials, ECyano@Fe_3O_4-M2pep was a "living material". As the incubation time prolonged, ECyano could proliferate. While the Fe_3O_4-M2pep nanoparticles could not reproduce, resulting in the decrease of Fe_3O_4-M2pep nanoparticles on the surface of ECyano. In the future work, we will use synthetic biology techniques to further modify strains, which can synthesize and release nanoparticles under the induction of theophylline, thus achieving the *in situ* production of PSs and nanoparticles.

4. Conclusion

In this paper, ECyano@Fe_3O_4-M2pep hybrid system was constructed as oxygen generator and photosensitizer production factory for synergistic cancer PDT-immunotherapy. Firstly, the modification of synthetic biology and Fe_3O_4-M2pep could not affect the photosynthetic capacity, laying the foundation for alleviating tumor hypoxia. Secondly, theophylline induced 5-ALA production could achieve the controlled and efficient PDT effects, which could prevent the premature killing of ECyano by ROS generated by PDT. Finally, Fe_3O_4-M2pep was released in response to the abundant ROS, targeted to M2-like TAMs, induced the polarization to M1-like TAMs and killed the tumor cells. The synergistic cancer PDT-immunotherapy could effectively relieve hypoxia, enhance the PDT effect, promote the polarization of M2-like TAMs and inhibit tumor growth. We believe that this hybrid system will offer a promising way for the biomedical application of bacterial therapy.

CRediT authorship contribution statement

Yize Li: Writing – original draft, Methodology, Formal analysis, Data curation. **Yali Fan:** Methodology, Investigation, Data curation. **Jin Gao:** Methodology, Investigation, Data curation. **Shaohui Zheng:** Writing – review & editing, Supervision, Investigation. **Yujuan Xing:** Investigation, Data curation. **Chunyan He:** Investigation, Data curation. **Shuo Ye:** Investigation, Data curation. **Hongfei Xia:** Investigation. **Gezhen Wang:** Investigation. **Hui Pan:** Investigation. **Wei Xia:** Investigation. **Meirong Sui:** Writing – review & editing, Supervision. **Hanjie Wang:** Writing – review & editing, Supervision. **Jing Liu:** Writing – review & editing, Supervision, Investigation. **Manman Xie:** Writing – review & editing, Supervision, Investigation. **Kai Xu:** Writing – review & editing, Supervision. **Yingying Zhang:** Writing – review & editing, Supervision, Project administration.

Declaration of competing interest

The authors declare that they have no known competing financial interests or personal relationships that could have appeared to influence the work reported in this paper.

Data availability

Data will be made available on request.

Acknowledgements

This work was sponsored by the National Natural Science Foundation of China (82302366), the Youth Fund Project of Natural Science Foundation of Jiangsu Province (BK20220663), the Fundamental Science Research Project of Jiangsu Province Colleges and Universities (22KJB310007), the Startup Fund for Youth Talent in Xuzhou Medical University (D2021029), the Integrated Innovation Project in Xuzhou Medical University (XYRHCX2021016) and Jiangsu Training Program of Innovation and Entrepreneurship for Undergraduates (202210313046Z).

Appendix A. Supplementary data

Supplementary data to this article can be found online at https://doi.org/10.1016/j.mtbio.2024.101192.

References

[1] T. Luo, Y. Fan, J. Mao, E. Yuan, E. You, Z. Xu, W. Lin, Dimensional reduction enhances photodynamic therapy of metal-organic nanophotosensitizers, J. Am. Chem. Soc. 144 (12) (2022) 5241–5246.
[2] Y. Yu, Q. Xu, S. He, H. Xiong, Q. Zhang, W. Xu, V. Ricotta, L. Bai, Q. Zhang, Z. Yu, J. Ding, H. Xiao, D. Zhou, Recent advances in delivery of photosensitive metal-based drugs, Coord. Chem. Rev. 387 (2019) 154–179.
[3] J. Zhang, N. Wang, Q. Li, Y. Zhou, Y. Luan, A two-pronged photodynamic nanodrug to prevent metastasis of basal-like breast cancer, Chem. Commun. 57 (18) (2021) 2305–2308.
[4] Y.-T. Fan, T.-J. Zhou, P.-F. Cui, Y.-J. He, X. Chang, L. Xing, H.-L. Jiang, Modulation of intracellular oxygen pressure by dual-drug nanoparticles to enhance photodynamic therapy, Adv. Funct. Mater. 29 (10) (2019).
[5] Z. Liu, T. Cao, Y. Xue, M. Li, M. Wu, J.W. Engle, Q. He, W. Cai, M. Lan, W. Zhang, Self-amplified photodynamic therapy through the $^1O_2$-mediated internalization of photosensitizers from a Ppa-bearing block copolymer, Angew. Chem. Int. Ed. 59 (9) (2020) 3711–3717.
[6] F. Wei, T.W. Rees, X. Liao, L. Ji, H. Chao, Oxygen self-sufficient photodynamic therapy, Coord. Chem. Rev. 432 (2021).
[7] S. Kumar, I.M. Adjei, S.B. Brown, O. Liseth, B. Sharma, Manganese dioxide nanoparticles protect cartilage from inflammation-induced oxidative stress, Biomaterials 224 (2019).
[8] S. Park, K.M. Park, Hyperbaric oxygen-generating hydrogels, Biomaterials 182 (2018) 234–244.
[9] H. Liao, Y. Cao, C. Hu, S. Shen, Z. Zhang, D. Li, Y. Du, Oxygen-producing and pH-responsive targeted DNA nanoflowers for enhanced chemo-sonodynamic therapy of lung cancer, Materials Today Bio 25 (2024).
[10] Y. Qiao, F. Yang, T. Xie, Z. Du, D. Zhong, Y. Qi, Y. Li, W. Li, Z. Lu, J. Rao, Y. Sun, M. Zhou, Engineered algae: a novel oxygen-generating system for effective treatment of hypoxic cancer, Sci. Adv. 6 (21) (2020).
[11] C. Gao, C.H.T. Kwong, Q. Wang, H. Kam, B. Xie, S.M.-Y. Lee, G. Chen, R. Wang, Conjugation of macrophage-mimetic microalgae and liposome for antitumor sonodynamic immunotherapy via hypoxia alleviation and autophagy inhibition, ACS Nano 17 (4) (2023) 4034–4049.
[12] T. Huokko, T. Ni, G.F. Dykes, D.M. Simpson, P. Brownridge, F.D. Conradi, R. J. Beynon, P.J. Nixon, C.W. Mullineaux, P. Zhang, L.-N. Liu, Probing the biogenesis pathway and dynamics of thylakoid membranes, Nat. Commun. 12 (1) (2021).
[13] D. Han, X. Zhang, Y. Ma, X. Yang, Z. Li, The development of live microorganism-based oxygen shuttles for enhanced hypoxic tumor therapy, Materials Today Bio 18 (2023).
[14] M. Huo, L. Wang, L. Zhang, C. Wei, Y. Chen, J. Shi, Photosynthetic tumor oxygenation by photosensitizer-containing cyanobacteria for enhanced photodynamic therapy, Angew. Chem. Int. Ed. 59 (5) (2020) 1906–1913.
[15] L. Liu, H. He, Z. Luo, H. Zhou, R. Liang, H. Pan, Y. Ma, L. Cai, In situ photocatalyzed oxygen generation with photosynthetic bacteria to enable robust immunogenic photodynamic therapy in triple-negative breast cancer, Adv. Funct. Mater. 30 (10) (2020).
[16] M. Huo, P. Liu, L. Zhang, C. Wei, L. Wang, Y. Chen, J. Shi, Upconversion nanoparticles hybridized cyanobacterial cells for near-infrared mediated photosynthesis and enhanced photodynamic therapy, Adv. Funct. Mater. 31 (16) (2021).
[17] H.J. Lee, J. Choi, S.-M. Lee, Y. Um, S.J. Sim, Y. Kim, H.M. Woo, Photosynthetic CO_2 conversion to fatty acid ethyl esters (FAEEs) using engineered cyanobacteria, J. Agric. Food Chem. 65 (6) (2017) 1087–1092.

[18] C. Tan, P. Xu, F. Tao, Carbon-negative synthetic biology: challenges and emerging trends of cyanobacterial technology, Trends Biotechnol. 40 (12) (2022) 1488–1502.
[19] J. Shi, W. Nie, X. Zhao, X. Yang, H. Cheng, T. Zhou, Y. Zhang, K. Zhang, J. Liu, An intracellular self-assembly-driven uninterrupted ROS generator augments 5-aminolevulinic-acid-based tumor therapy, Adv. Mater. 34 (30) (2022).
[20] A. Mantovani, F. Marchesi, A. Malesci, L. Laghi, P. Allavena, Tumour-associated macrophages as treatment targets in oncology, Nat. Rev. Clin. Oncol. 14 (7) (2017) 399–416.
[21] X. Xiang, J. Wang, D. Lu, X. Xu, Targeting tumor-associated macrophages to synergize tumor immunotherapy, Signal Transduct. Targeted Ther. 6 (1) (2021).
[22] Y. Huang, Z. Guan, X. Dai, Y. Shen, Q. Wei, L. Ren, J. Jiang, Z. Xiao, Y. Jiang, D. Liu, Z. Huang, X. Xu, Y. Luo, C. Zhao, Engineered macrophages as near-infrared light activated drug vectors for chemo-photodynamic therapy of primary and bone metastatic breast cancer, Nat. Commun. 12 (1) (2021).
[23] X. Li, G. Chen, Y. Wang, L. Su, B. Chen, K. Wu, Y. Xing, Z. Song, R. Dai, T. Liu, J. Zhao, Z. Xie, P. Zhou, X. Xia, Y. Min, Systematic co-delivery of dual agonists to enhance cancer immunotherapy, Nano Res. 15 (9) (2022) 8326–8335.
[24] Y. Lin, X. Wang, S. He, Z. Duan, Y. Zhang, X. Sun, Y. Hu, Y. Zhang, Z. Qian, X. Gao, Z. Zhang, Immunostimulatory gene therapy combined with checkpoint blockade reshapes tumor microenvironment and enhances ovarian cancer immunotherapy, Acta Pharm. Sin. B 14 (2) (2024) 854–868.
[25] S. Zanganeh, G. Hutter, R. Spitler, O. Lenkov, M. Mahmoudi, A. Shaw, J. S. Pajarinen, H. Nejadnik, S. Goodman, M. Moseley, L.M. Coussens, H.E. Daldrup-Link, Iron oxide nanoparticles inhibit tumour growth by inducing pro-inflammatory macrophage polarization in tumour tissues, Nat. Nanotechnol. 11 (11) (2016) 986–994.
[26] S. Li, T. Sun, C. Xu, L. Chen, W. Zhang, Development and optimization of genetic toolboxes for a fast-growing cyanobacterium *Synechococcus elongatus* UTEX 2973, Metab. Eng. 48 (2018) 163–174.
[27] M. Xie, Z. Wang, Q. Lu, S. Nie, C.J. Butch, Y. Wang, B. Dai, Ultracompact iron oxide nanoparticles with a monolayer coating of succinylated heparin: a new class of renal-clearable and nontoxic T_1 agents for high-field MRI, ACS Appl. Mater. Interfaces 12 (48) (2020) 53994–54004.
[28] Y. Nakahira, A. Ogawa, H. Asano, T. Oyama, Y. Tozawa, Theophylline-dependent riboswitch as a novel genetic tool for strict regulation of protein expression in cyanobacterium *Synechococcus elongatus* PCC 7942, Plant Cell Physiol. 54 (10) (2013) 1724–1735.
[29] T. Sun, S. Li, X. Song, G. Pei, J. Diao, J. Cui, M. Shi, L. Chen, W. Zhang, Re-direction of carbon flux to key precursor malonyl-CoA via artificial small RNAs in photosynthetic *Synechocystis* sp PCC 6803, Biotechnol. Biofuels 11 (2018).
[30] T. Sun, Y. Zhang, C. Zhang, H. Wang, H. Pan, J. Liu, Z. Li, L. Chen, J. Chang, W. Zhang, Cyanobacteria-Based bio-oxygen pump promoting hypoxia-resistant photodynamic therapy, Front. Bioeng. Biotechnol. 8 (2020).
[31] Z. Sun, M. Zhao, W. Wang, L. Hong, Z. Wu, G. Luo, S. Lu, Y. Tang, J. Li, J. Wang, Y. Zhang, L. Zhang, 5-ALA mediated photodynamic therapy with combined treatment improves anti-tumor efficacy of immunotherapy through boosting immunogenic cell death, Cancer Lett. 554 (2023).
[32] D. Zhong, J. Li, W. Ma, H. Xin, Magnetite nanoparticles enhanced glucose anaerobic fermentation for bio-hydrogen production using an expanded granular sludge bed (EGSB) reactor, Int. J. Hydrogen Energy 45 (18) (2020) 10664–10672.
[33] J.J. Mistry, C.R. Marlein, J.A. Moore, C. Hellmich, E.E. Wojtowicz, J.G.W. Smith, I. Macaulay, Y. Sun, A. Morfakis, A. Patterson, R.H. Horton, D. Divekar, C.J. Morris, A. Haestier, F. Di Palma, N. Beraza, K.M. Bowles, S.A. Rushworth, ROS-mediated PI3K activation drives mitochondrial transfer from stromal cells to hematopoietic stem cells in response to infection, Proc. Natl. Acad. Sci. U.S.A. 116 (49) (2019) 24610–24619.